



Pacific Northwest
NATIONAL LABORATORY

Proudly Operated by Battelle Since 1965

High-Resolution Characterization of UMo Alloy Microstructure

November 2016

A Devaraj
VV Joshi
S Manandhar
CA Lavender

L Kovarik
S Jana
BW Arey

DISCLAIMER

This report was prepared as an account of work sponsored by an agency of the United States Government. Neither the United States Government nor any agency thereof, nor Battelle Memorial Institute, nor any of their employees, makes **any warranty, express or implied, or assumes any legal liability or responsibility for the accuracy, completeness, or usefulness of any information, apparatus, product, or process disclosed, or represents that its use would not infringe privately owned rights.** Reference herein to any specific commercial product, process, or service by trade name, trademark, manufacturer, or otherwise does not necessarily constitute or imply its endorsement, recommendation, or favoring by the United States Government or any agency thereof, or Battelle Memorial Institute. The views and opinions of authors expressed herein do not necessarily state or reflect those of the United States Government or any agency thereof.

PACIFIC NORTHWEST NATIONAL LABORATORY
operated by
BATTELLE
for the
UNITED STATES DEPARTMENT OF ENERGY
under Contract DE-AC05-76RL01830

Printed in the United States of America

Available to DOE and DOE contractors from the
Office of Scientific and Technical Information,
P.O. Box 62, Oak Ridge, TN 37831-0062;
ph: (865) 576-8401
fax: (865) 576-5728
email: reports@adonis.osti.gov

Available to the public from the National Technical Information Service
5301 Shawnee Rd., Alexandria, VA 22312
ph: (800) 553-NTIS (6847)
email: orders@ntis.gov <<http://www.ntis.gov/about/form.aspx>>
Online ordering: <http://www.ntis.gov>



This document was printed on recycled paper.

(8/2010)

High-Resolution Characterization of UMo Alloy Microstructure

A Devaraj
VV Joshi
S Manandhar
CA Lavender

L Kovarik
S Jana
BW Arey

November 2016

Prepared for
the U.S. Department of Energy
under Contract DE-AC05-76RL01830

Pacific Northwest National Laboratory
Richland, Washington 99352

Executive Summary

Uranium-molybdenum (UMo) fuel processing steps, from casting to forming final fuel, directly affect the microstructure of the fuel, which in turn dictates the in-reactor performance of the fuel under irradiation. In order to understand the influence of processing on UMo microstructure, microstructure characterization techniques are necessary. When microstructural features approach submicron size scales, they become harder to detect and quantitatively analyze by conventional characterization techniques like optical microscopy or scanning electron microscopy or X-ray diffraction. In such instances, higher resolution characterization techniques like transmission electron microscopy (TEM) and atom probe tomography (APT) are needed to interrogate the details of the microstructure. The findings from TEM and APT are also directly beneficial for developing predictive multiscale modeling tools that can predict the microstructure as a function of process parameters. This report provides background on focused-ion-beam-based TEM and APT sample preparation, TEM and APT analysis procedures, and the unique information achievable through such advanced characterization capabilities for UMo fuels, from a fuel fabrication capability viewpoint.

Acronyms and Abbreviations

APT	atom probe tomography
C	carbon
EDS	energy-dispersive x-ray spectroscopy
FFT	fast Fourier transform
FIB	focused ion beam
Ga	gallium
GIS	gas-injection system
HRSTEM	high-resolution scanning transmission electron microscopy
Mo	molybdenum
OM	optical microscopy
PNNL	Pacific Northwest National Laboratory
Pt	platinum
SAD	selected area diffraction
SEM	scanning electron microscopy
STEM	scanning transmission electron microscopy
TEM	transmission electron microscopy
U	uranium
U-10Mo	uranium alloyed with 10 weight percent molybdenum
UMo	body-centered cubic γ -UMo
XRD	x-ray diffraction

Units

°C	degree(s) Celsius
μm	micrometer(s)
Da	dalton(s)
kV	kilovolt(s)
nA	nanoampere(s)
nJ	nanojoule(s)
pA	picoampere(s)
pJ	picojoule(s)
wt%	weight percent

Contents

Executive Summary	iii
Acronyms and Abbreviations	v
1.0 Introduction	1
2.0 Metallographic Preparation of Samples.....	2
3.0 FIB-Based Preparation of Specimens for TEM and APT.....	2
3.1 FIB-Based Preparation of TEM Samples.....	2
3.2 FIB-Based Preparation of APT Samples.....	5
4.0 TEM Imaging and Diffraction Procedure.....	6
5.0 APT Analysis Procedure	11
6.0 Conclusions	14
7.0 Recommendations	15
8.0 References	15

Figures

1	Imaging Equipment	2
2	FIB Preparation of TEM Samples with Specific Carbides from 1000°C-60 h Annealed U-10Mo Alloy	4
3	TEM Sample Preparation of a Transformed Region of a 500°C-10 h Isothermally Annealed U-10Mo Alloy	5
4	FIB-Based Preparation of APT Needle Samples from a Transformed Area of U-10Mo	6
5	Crystal Structure Model and SAD Simulations of γ -U-10Mo	7
6	Crystal Structure Model and SAD Simulations of α -U	8
7	Crystal Structure Model and SAD Simulations of γ' -U ₂ Mo	8
8	Crystal Structure Model and SAD Simulations of UC	9
9	Crystal Structure Model and SAD Simulations of MoSi ₂	9
10	TEM Analysis of Homogenized U-10Mo Alloy	10
11	Transformed Lamellar Microstructure in 500°C-10 h Isothermally Annealed U-10Mo alloy	11
12	Schematics of APT Technique and Reconstructed Result	13
13	Carbides in As-Cast U-10Mo Alloy	13
14	Transformed Regions in a U-10Mo Alloy Isothermally Aged at 500°C for 10 Hours	14

Tables

1	Space Group and Lattice Parameters of Various Ideal Phases in U-10Mo Alloy System	7
---	---	---

1.0 Introduction

The Fuel Fabrication Capability pillar of the U.S. Department of Energy National Nuclear Security Administration's Reactor Conversion Program is focused on developing a streamlined fuel manufacturing method. Doing so will require increased understanding of the effects of processing conditions on the final fuel microstructure. During the entire process flow—from casting to final fuel form—uranium alloyed with 10 wt% molybdenum (U-10Mo) is subjected to different time-temperature histories and mechanical deformations. Hence, body-centered cubic gamma uranium-molybdenum (UMo) alloy microstructure continuously evolves as it is subjected to different steps in the process to convert it from as-cast microstructure to final fuel foil. The microstructure of the UMo alloy has a direct influence on the selection of processing parameters for all stages of processing, and it will dictate the final fuel microstructure and hence the irradiation response once in a reactor. The program is also developing a robust modeling capability that can help predict the microstructure development as a function of processing, for which detailed microstructural characterization needs to be performed. Hence, it is imperative to develop a detailed understanding of UMo fuel microstructure as the fuel fabrication capability is developed, so that a predictable microstructure can be consistently achieved. To address this need, we have been developing a detailed understanding of changes in UMo microstructure from as-cast state to final fuel form. This report will serve to document the characterization methods used by the characterization working group.

The microstructure characterization starts with optical microscopy (OM), scanning electron microscopy (SEM), and x-ray diffraction (XRD). These techniques reach their limit of sensitivity as the microstructural features in UMo approach submicron size scales. Complementing the data generated by SEM, OM, and XRD with other techniques is frequently needed in the initial stages of process development. For example, during homogenization, the carbides undergo spheroidization that may be associated with solute exchange between the carbide and matrix, which is not easily detectable by OM, SEM, or XRD. Another example is the eutectoid transformation during hot isostatic processing, which develops lamellar microstructure in which individual lamellae are often of submicron size, which limits the usefulness of conventional SEM–energy-dispersive x-ray spectroscopy (EDS) methods to evaluate the composition of individual lamellae. An example for this case is given in section 5 of a recent report (Devaraj et al. 2016), which highlights the inability of only OM or XRD to detect the type of transformation product. Another example is given in sections 3.2 and 3.3 of Jana et al. (2016), where the composition and structure of transformation products formed during isothermal annealing at 400°C and 500°C are difficult to understand without using transmission electron microscopy (TEM) or atom probe tomography (APT) analysis in addition to OM, SEM imaging, or XRD analysis. To meet these needs, we have employed high-resolution characterization techniques, namely aberration-corrected TEM and APT, in conjunction with focused ion beam (FIB) techniques to develop a comprehensive understanding of the UMo microstructure. The instruments are shown in Figure 1. This report will serve as the one-stop reference for the procedures for using the advanced characterization methods in conjunction with more conventional microstructure characterization methods for UMo alloys.

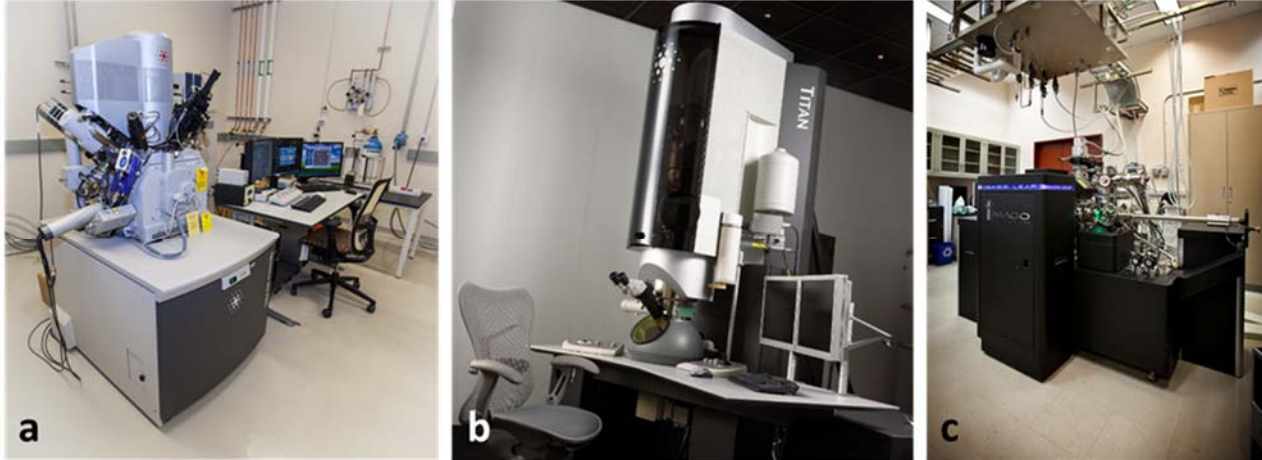


Figure 1. High resolution characterization Equipment. (a) The radiological FEI Quanta 3D FIB-SEM; (b) the FEI 300 kV Titan aberration-corrected monochromated scanning transmission electron microscope; (c) the CAMECA LEAP 4000X-HR APT system available at the Environmental Molecular Sciences Laboratory at Pacific Northwest National Laboratory (PNNL).

2.0 Metallographic Preparation of Samples

Metallographic polishing of UMo samples has been discussed in detail in a report by Prabhakaran et al. (2016), which deals with detailed procedures for mounting and metallographic polishing. All specimens described here were prepared consistently using the same methods. Mounted and polished samples are kept in safe storage locations between experiments to minimize accumulation of contamination on specimen surfaces.

3.0 FIB-Based Preparation of Specimens for TEM and APT

3.1 FIB-Based Preparation of TEM Samples

TEM samples are prepared from mounted and metallographically polished bulk specimens of UMo. The step-by-step procedure for preparing a TEM sample using an FEI dual-beam FIB-SEM system equipped with Omniprobe nanomanipulator and Pt- or C-gas-injection system (GIS) is given below.

1. SEM imaging is used to select a specific region of interest (ROI), such as UC precipitates or a transformed region near a grain boundary (See Figure 2a for an example of selecting an ROI with two carbides).
2. Then the ROI is coated with electron-beam assisted Pt deposition using the Pt-GIS first, followed by ion-beam assisted Pt deposition on top of the same region. The electron-beam assisted Pt deposition area is typically around 10-20 μm long, 1-2 μm wide, and 100-300 nm thick. Electron-beam assisted Pt deposition can be carried out at either 30 kV or 5 kV with greater than 4 nA beam current. Thereafter, a much thicker (approximately 1.5-2 μm thick) Pt cap is deposited using ion-beam assisted Pt deposition (Figure 2b). For ion-beam assisted Pt deposition, 30 kV acceleration voltage and 49 pA Ga ion beam current is used.
3. After deposition of the Pt cap, the specimen stage is tilted to 52° to make the sample surface perpendicular to the ion beam.

4. Two rectangular trenches are made, one on either side of the Pt protected region, to define a thin lamella approximately 1 μm wide. This trenching is performed using an ion beam at 30 kV acceleration voltage and 3 nA current. The trenches on either side of the lamella are kept at least 4 μm wide, about 1 micron longer than the Pt protected ROI on either side, and depth of milling is maintained at greater than 5 μm depending upon the thickness of the TEM sample to be made.
5. Then the stage is tilted back to 0° to perform a “U”-shaped undercut of the lamella, leaving about 15 μm width for the TEM sample. Undercutting is typically done using 1 nA current at 30 kV acceleration voltage of the Ga ion beam. During undercutting, a small extension of the sample is left uncut on each end to keep it attached to the bulk sample until the next step is completed.
6. Then the Omniprobe nanomanipulator is inserted and brought into contact with the lamella. Using the Pt-GIS, the Omniprobe is then welded onto the thin lamella by using a 30 kV-49 pA ion-beam current. Then the small attachments on either end are cut to free the lamella from the bulk sample using 30 kV-1 nA current.
7. The detached sample lamella is lifted-out of the trench and it is attached onto a Cu TEM grid post using 30 kV-49 pA ion-beam current Pt deposition.
8. The TEM grid stage is tilted to 52° and it is initially thinned in 5 μm sized window regions using 30 kV-0.5 nA ion-beam current until the width becomes \sim 600 nm at the top.
9. The TEM lamella is tilted to 56° for one side and 48° for the other side, and progressively thinned using cleaning cross-section milling on either side using 30 kV-49 pA current until a thin region is formed, as visible from SEM images (Figure 2c).
10. Then the acceleration voltage is reduced to 2 kV and thinning is continued at 49 pA until a hole forms near a very thin region. Uranium mills very slowly during ion-beam milling, so often it is very difficult to get uniform thin regions with electron transparency but without holes (Figure 2d).

A similar approach is used for preparing TEM samples of transformed microstructures as shown in Figure 3.

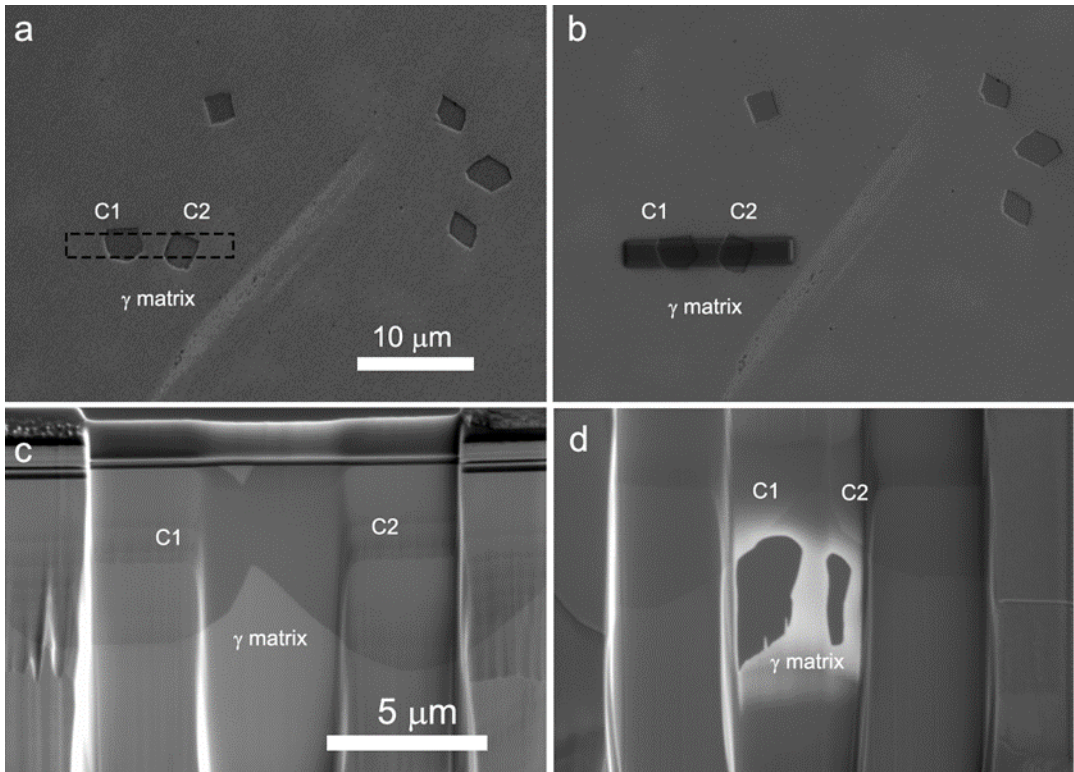


Figure 2. FIB Preparation of TEM Samples with Specific Carbides from 1000°C-60 h Annealed U-10Mo Alloy. The two carbides selected for the TEM samples are shown as C1 and C2. (a) the ROI; (b) after Pt deposition on the ROI; (c) the lift-out TEM lamella after initial thinning (d) the TEM lamella after final low-kV cleaning showing thin regions beside holes.

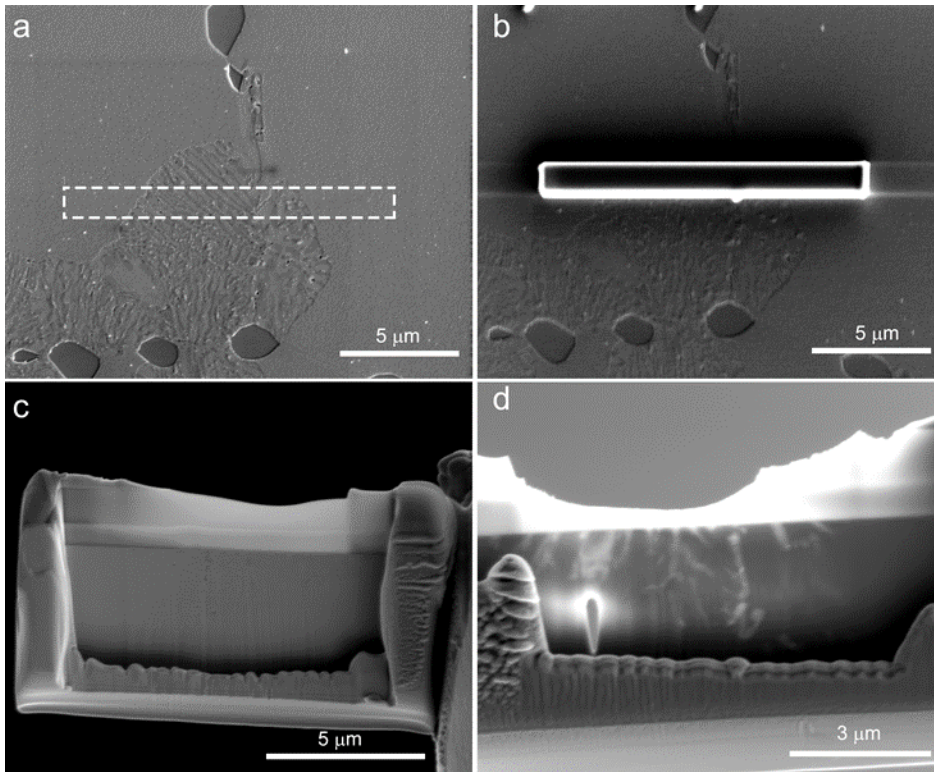


Figure 3. TEM Sample Preparation of a Transformed Region of a 500°C-10 h Isothermally Annealed U-10Mo Alloy. (a) the ROI; (b) after Pt deposition on the ROI; (c) TEM sample lamella after initial thinning; (d) final TEM lamella after final thinning, showing the transformed regions.

3.2 FIB-Based Preparation of APT Samples

A FIB-based site-specific lift-out procedure is used to make APT specimens from different microstructural features of U-10Mo alloy samples. Figure 4 shows the steps involved in preparing an APT needle specimen.

1. A transformed region within 500°C-10 h annealed U-10Mo is selected as the ROI (Figure 4a).
2. The ROI is protected with electron-beam assisted Pt deposition and then ion-beam assisted Pt deposition as shown in Figure 4b; typically the length of Pt deposition is 12-16 μm , the width is 1.2 μm , and thickness is about 1 μm .
3. The sample is tilted to 22° and two trenches are cut, one on either side of the Pt coated region, to create a wedge shaped sample (Figure 4c).
4. This wedge shaped sample is extracted using the Omniprobe nanomanipulator and attached to a commercially purchased silicon microtip array sample holder (Figure 4d).
5. A roughly 2 μm sized section of one lift-out wedge 12 μm length, is successively attached to the tops of six different microtip array posts. One such piece of the lift-out is shown in Figure 4e.
6. This wedge is then subjected to annular milling by a 30 kV Ga ion beam to sharpen it to the final needle shape (Figure 4f).

7. The sharpened needle is further cleaned using a 2 kV Ga ion beam to achieve a final needle specimen with very minimal Ga contamination or surface damage as shown in Figure 4g.
8. After all needles are sharpened, the microtip array is loaded into a shuttle box and transferred to the APT vacuum load lock with minimal exposure to air.

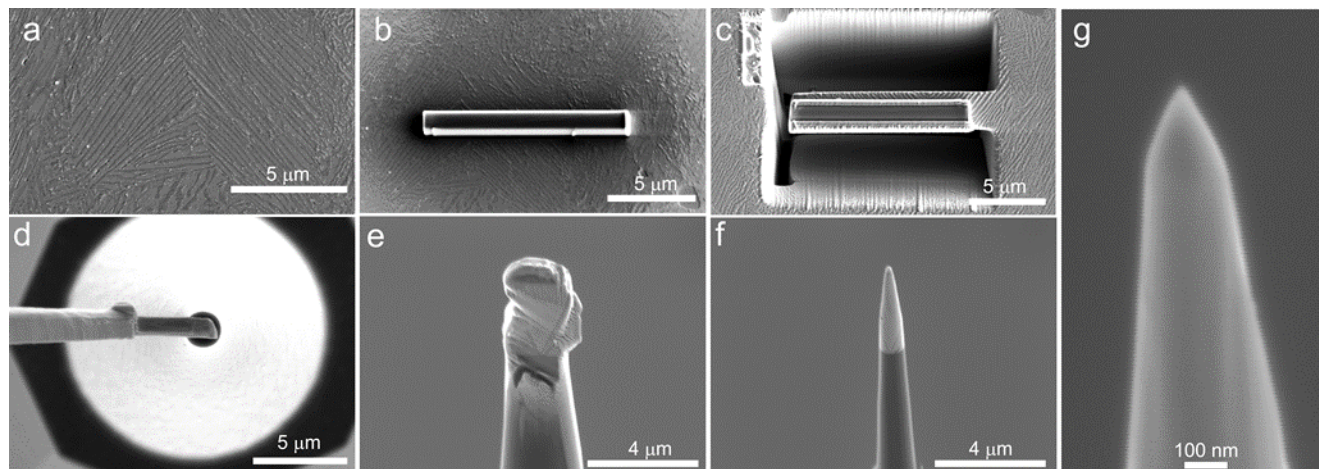


Figure 4. FIB-Based Preparation of APT Needle Samples from a Transformed Area of U-10Mo

4.0 TEM Imaging and Diffraction

The TEM specimens in this work were imaged using a 300 kV aberration-corrected FEI Titan scanning transmission electron microscope (STEM). TEM bright field images provide an overall high-magnification image of all the different features in the sample. The selected area diffraction (SAD) patterns collected from individual features in the sample provide the crystallographic information for each of the microstructural features. High-angle annular dark field-STEM imaging (HAADF-STEM) was also used to obtain atomic mass contrast in images, which is useful to get qualitative information on the composition of different microstructural features in addition to their structure. In order to confirm the structure of various microstructural features in U-10Mo, the experimentally collected SAD patterns of ideal structures of various phases were compared with simulated SAD patterns. The SAD simulations were done with SingleCrystal software using the space group, lattice parameters, and site occupancy information obtained from the Inorganic Crystal Structure Database (ICSD), as shown in Table 1. The SAD simulations were conducted for the most common zone axes, namely [100] type directions and [110] and [111] zone axes for all common phases present in U-10Mo alloys.

Crystal structure model and simulated SAD patterns for all major zone axes are shown in the following figures: γ -U-10Mo (Figure 5), α -U (Figure 6), γ' -U₂Mo (Figure 7), UC (Figure 8) and MoSi₂ (Figure 9). During experimental TEM analysis of UMo alloy samples, all the experimentally collected SAD patterns were compared with these simulated data sets to verify whether the expected structures are formed in the U-10Mo alloy or new phases are formed. In instances where a variation in experimental SAD patterns from these simulated SAD patterns was observed, we delved into further detailed analysis to understand the root cause for deviation from already reported structures and compositions. We then linked those new findings to mass-balance calculations that are critical for determining acceptable tolerances for alloy composition specification, which in turn can influence process parameters. We have also investigated the interfaces between all these phases to understand the structural coherency between these phases and the presence or absence of any orientation relationships between the phases using TEM or high-resolution STEM (HRSTEM) imaging. Such structural coherency can play a crucial role in determining precipitate fracture during rolling or other mechanical processing steps. The structural

coherency can also change the interfacial energy, which affects the reliability of phase field simulations being developed for predicting the microstructure of U-10Mo alloys.

Table 1. Space Group and Lattice Parameters of Various Ideal Phases in U-10Mo Alloy System

Phase	Space Group	Lattice Parameter (Å)
γ -U-10Mo	I m-3m	a = 3.41
α -U	C m c m	a = 2.85 b = 5.85 c = 4.95
γ' -U ₂ Mo	I 4/m m m	a = 3.427 c = 9.834
UC	F m -3 m	a = 4.96
MoSi ₂	I 4/m m m	a = 3.2 c = 7.861

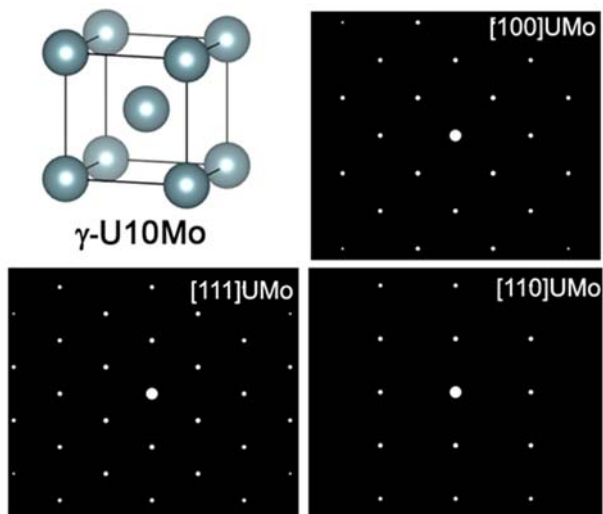


Figure 5. Crystal Structure Model and SAD Simulations of γ -U-10Mo

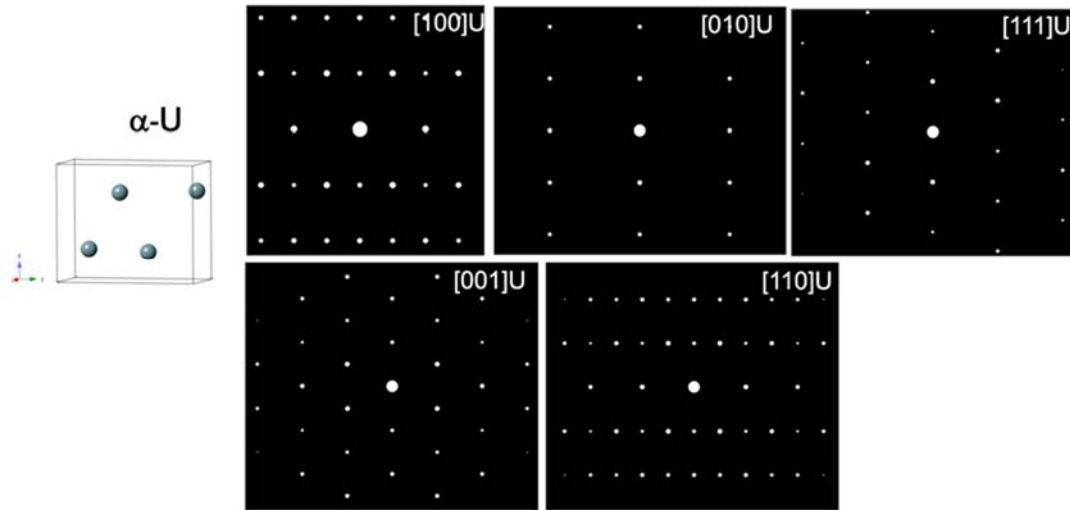


Figure 6. Crystal Structure Model and SAD Simulations of α -U

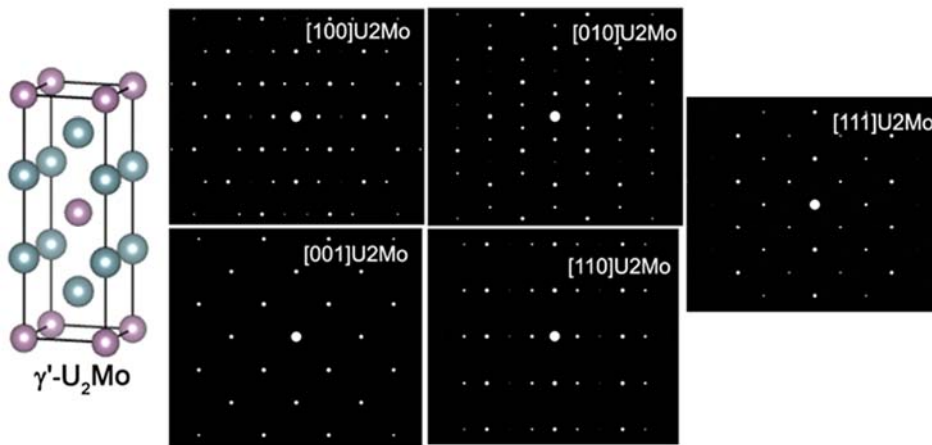


Figure 7. Crystal Structure Model and SAD Simulations of γ' -U₂Mo

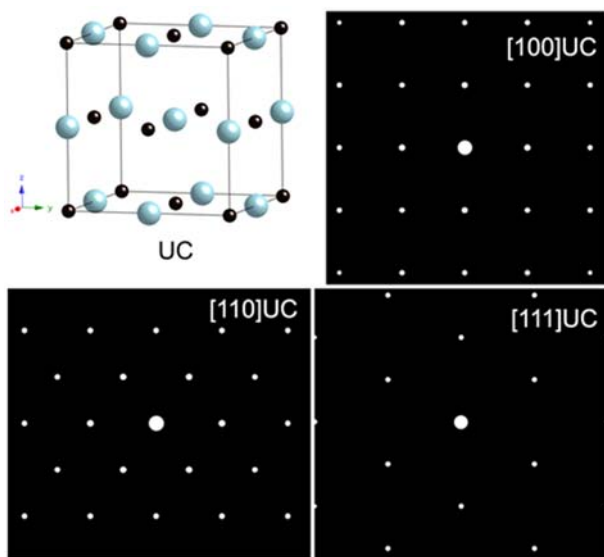


Figure 8. Crystal Structure Model and SAD Simulations of UC

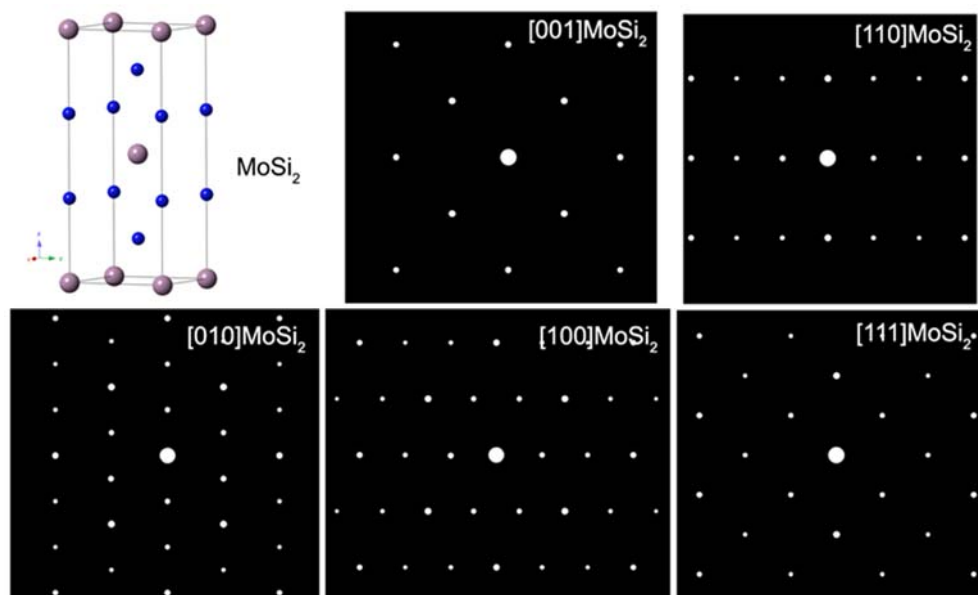


Figure 9. Crystal Structure Model and SAD Simulations of MoSi₂

Two representative examples for advanced TEM analysis of UMo alloys are given in Figure 10 and Figure 11. Figure 10a shows a STEM image of a uranium carbide and the surrounding γ -UMo matrix in a 900°C-48 h homogenized U-10Mo alloy. The SAD patterns from both phases are shown in Figure 10b, and the HRSTEM image and corresponding fast Fourier transform (FFT) patterns of both phases are shown in Figure 10c. Such detailed analysis has been conducted to understand the structure of UC and the UMo matrix as well as Si-rich precipitates as a function of homogenization temperature and time. The second example, in Figure 11, is of detailed TEM analysis of a lamellar microstructure in a transformed region of a U-10Mo alloy isothermally annealed at 500°C for 10 h. Figure 11a shows a STEM image of the lamellar region with the region chosen for SAD analysis highlighted by a dashed circle. The SAD pattern shown in Figure 11b highlights the presence of γ -UMo in the interlamellar region. The HRSTEM images of the lamellar region in Figure 11c and Figure 11d highlight the detailed structural analysis of the interface between the two lamellae. It is to be noted that such

detailed understanding of impurity phases and transformation products is absolutely necessary to understand the evolving microstructure of U-10Mo alloys during the fuel fabrication process.

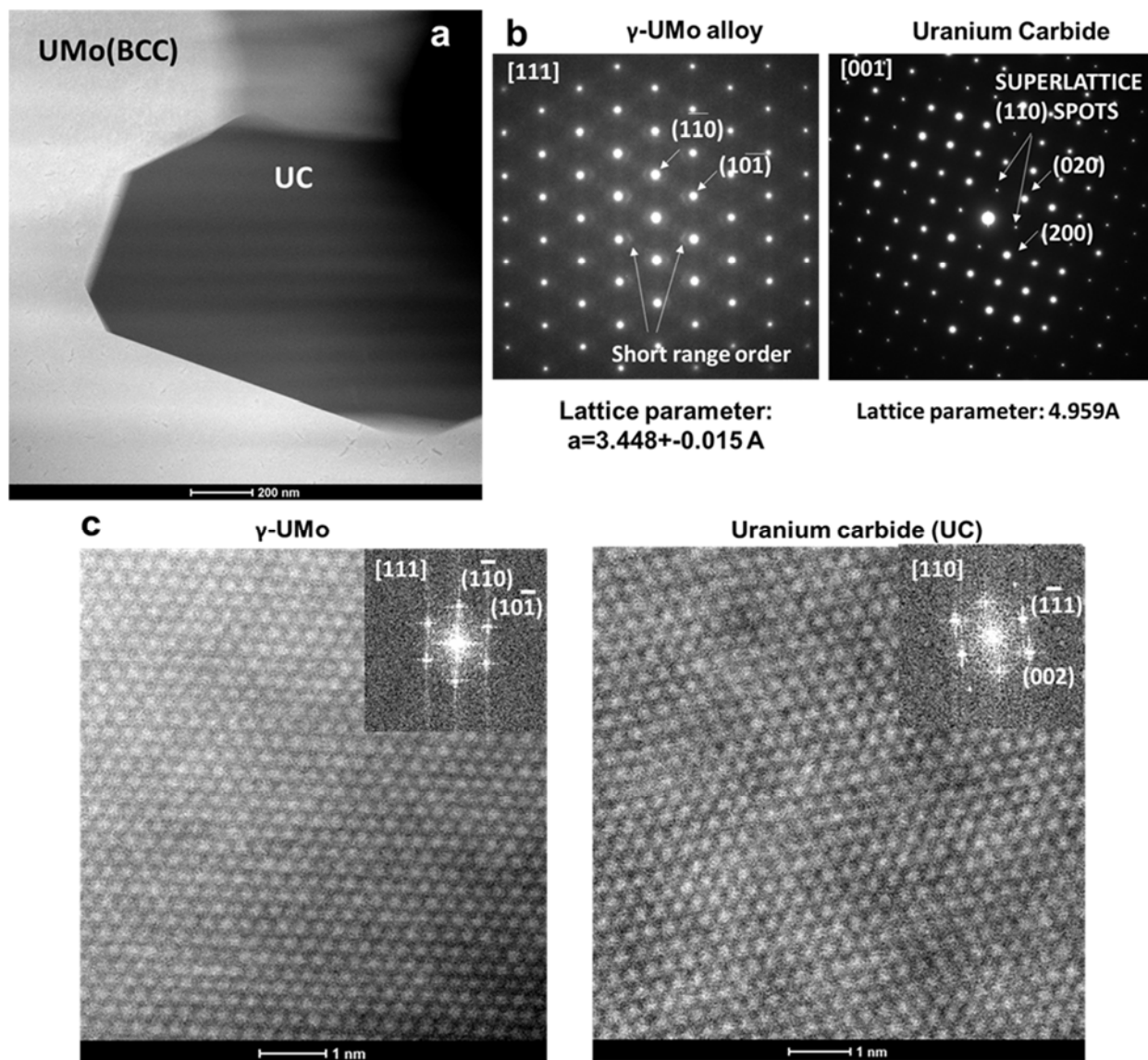


Figure 10. TEM Analysis of Homogenized U-10Mo Alloy. (a) STEM image of U-10Mo alloy homogenized for 48 h at 900°C showing carbide and γ -Umo matrix; (b) SAD patterns of γ -Umo matrix and UC; (c) HRSTEM image of γ -Umo matrix and UC with corresponding FFT patterns as insets.

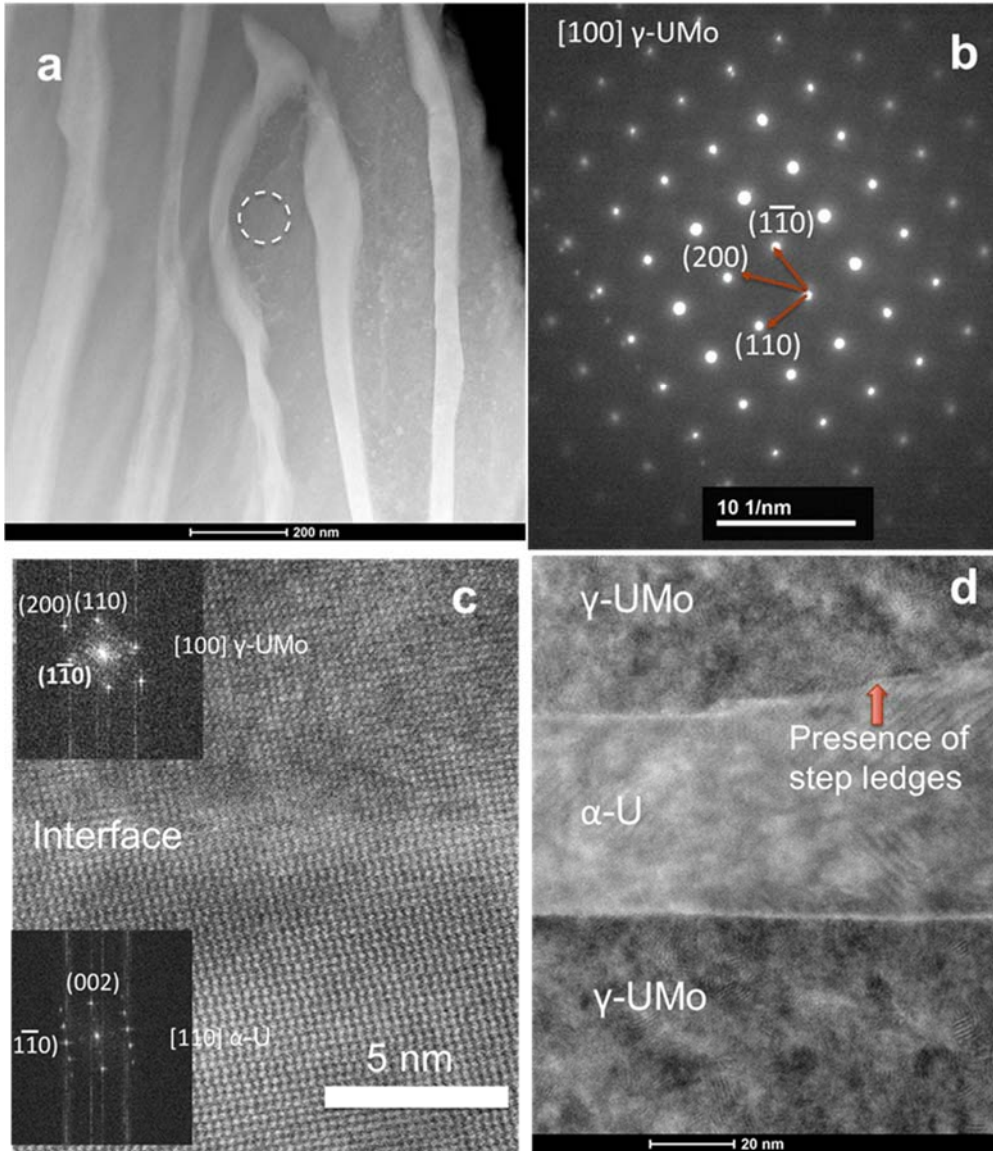


Figure 11. Transformed Lamellar Microstructure in 500°C-10 h Isothermally Annealed U-10Mo alloy. (a) STEM HAADF image; the region selected for SAD is highlighted by the dashed circle. (b) SAD pattern showing presence of γ -Umo in the darker lamellar region in STEM image; (c) HRSTEM image showing the interface between γ -Umo and α -U lamella; (d) HRSTEM imaging showing presence of step ledges between the lamellae.

5.0 APT Analysis Procedure

Atom probe tomography is used to analyze the nanoscale composition of all different features in the microstructure of U-10Mo alloy. Note that techniques like SEM-EDS have a large interaction volume with the electron beam and hence it is very difficult to analyze the composition of different phases, especially at nanoscale spatial resolution. EDS-based techniques (even in TEM-EDS) are semiquantitative and rely on how the data is being analyzed by the operator; the energy peaks of several elements often overlap with each other, and appropriate analysis techniques need to be used. In order to verify the exact composition, APT is often used and

complements the EDS or other chemical analysis techniques. For example, as-cast and homogenized U-10Mo contains impurity phases like UC and Si-rich precipitates, and with stand-alone SEM-EDS it is impossible to check the composition of these phases or understand the compositional change at their interface with the UMo matrix. Another example is that, after transformation by isothermal annealing at temperatures near 400-500°C, the transformation products are often lamellar, with individual lamella dimensions in tens to hundreds of nanometers. When individual lamellae are submicron size, SEM-EDS often has large interaction volumes that average the concentration of multiple lamellae, making it impossible to obtain the composition of individual lamellae from SEM-EDS alone. Based on published literature, there are multiple possible phase transformation pathways for decomposition of gamma-phase UMo during isothermal annealing, which makes it even more important to clearly understand the composition and structure of transformation products [S. Jana et al., 2016]. For all these reasons, APT is crucial for analyzing UMo alloy microstructure.

A schematic illustrating the basic operation of APT is provided in Figure 12. For APT, a needle-shaped specimen is made from the microstructural feature of interest, as shown in Figure 4, and loaded in an ultrahigh-vacuum chamber. The sample temperature is brought to 50 K, and a high electric field of the order of tens of volts per nanometer is applied on the needle specimen along with a pulsed ultraviolet (UV) laser focused on the specimen apex. The combined effect of the UV laser and the applied electric field facilitates controlled field evaporation and ionization of atoms of the U-10Mo alloy, which fly toward the detector along the electric field lines and reach a position-sensitive detector that measures both the x and y positions of ions as well as their times of flight. Using time of flight, the mass-to-charge ratios of all ions are calculated; these, along with the (x, y) position from the detector and the z information from the sequence of evaporation are used for reconstructing the atom positions in the microstructure of the material.

The APT analysis in this work was conducted using the CAMECA LEAP 4000X-HR atom probe system equipped with a 355 nm UV laser at the Environmental Molecular Sciences Laboratory at PNNL. The laser pulse energy was kept constant at 100 pJ and the specimen was kept at 50 K throughout the analysis. The evaporation rate was maintained at 0.005 atoms/pulse with a 100 kHz pulse repetition rate. The APT data was analyzed using Interactive Visualization and Analysis Software (IVAS) from CAMECA. During APT data reconstruction, a SEM image of the final needle specimen was used to accurately reconstruct the material. The mass-to-charge ratio ranging was done to accurately index all elemental and molecular peaks of U, Mo, and impurity elements like C, Si, Al, and O.

Two examples of typical APT results from U-10Mo alloys are shown here. In Figure 13a, the SEM image of carbides in an as-cast U-10Mo alloy is provided; Figure 13b is the final SEM image of a needle specimen containing the γ -UMo-UC interface, and Figure 13c is the APT reconstruction of the γ -UMo-UC highlighting the segregation of Si at the interface. The mass-to-charge ratio spectrum of the same needle specimen including both UMo matrix and UC regions is shown in Figure 13d. Figure 14a shows the SEM image of transformed regions in a U-10Mo alloy isothermally annealed at 500°C for 10 hours from which APT needle specimens were prepared. The final APT reconstruction is shown in Figure 14b. The composition partitioning between the γ -UMo and α -U, estimated using proximity histogram analysis, is shown in Figure 14c. Figure 14d shows the typical mass-to-charge ratio spectrum from APT results of transformed microstructural regions.

APT uniquely provides accurate compositional analysis of various phases in the microstructure of U-10Mo alloys, of not only major elements but also minor impurity elements. The results, when correlated with structural analysis by TEM and lower magnification imaging by SEM and OM, can help in developing a comprehensive understanding of the microstructural evolution at various stages of U-10Mo processing during fuel fabrication.

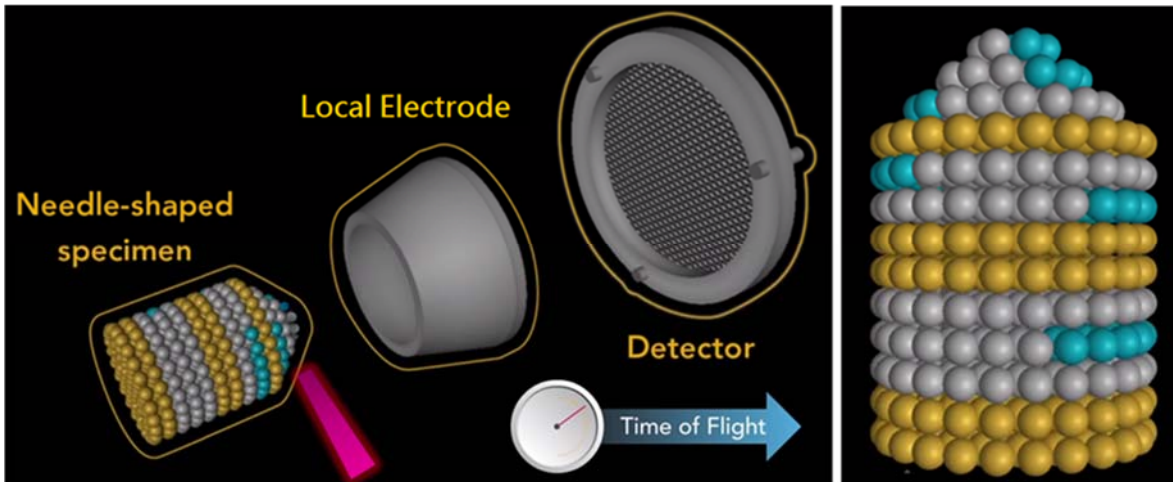


Figure 12. Schematics of APT Technique and Reconstructed Result

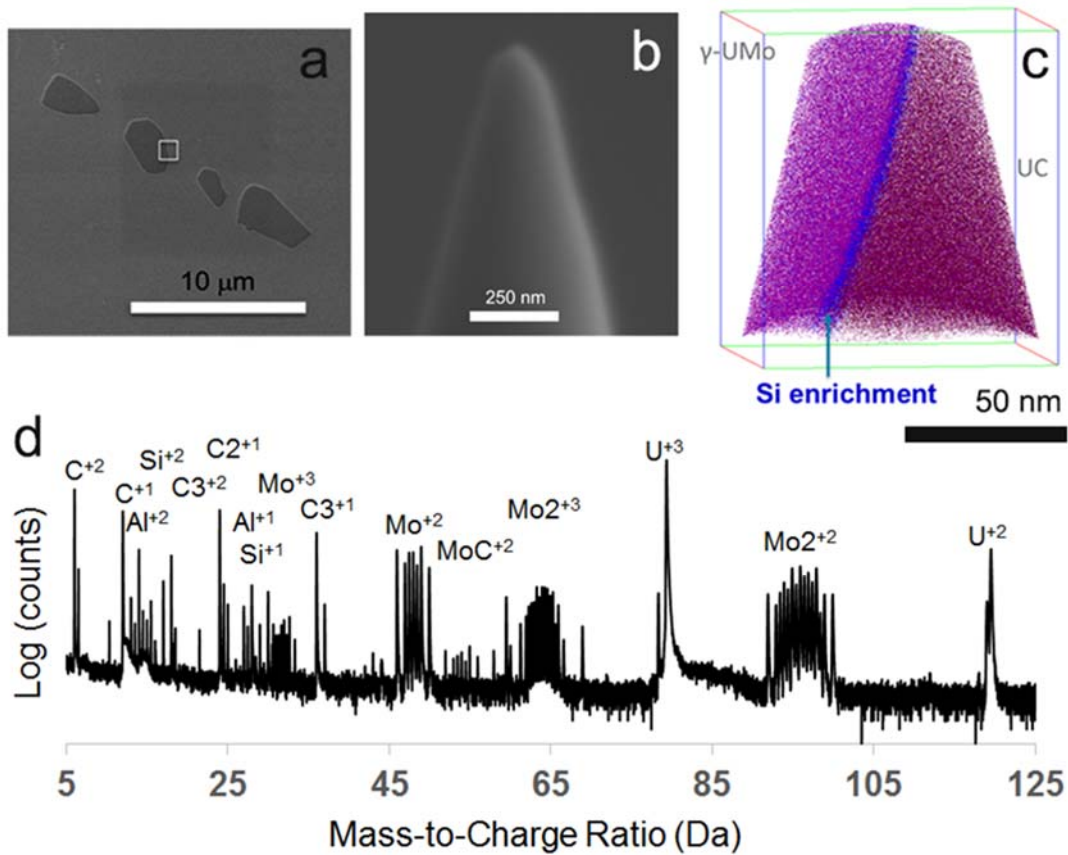


Figure 13. Carbides in As-Cast U-10Mo Alloy. SEM images of (a) carbides and (b) needle specimen; (c) the corresponding APT reconstruction showing the regions of γ -UMo and UC with Si enrichment at the interface between them; (d) The mass-to-charge ratio spectrum of the same atom probe reconstruction.

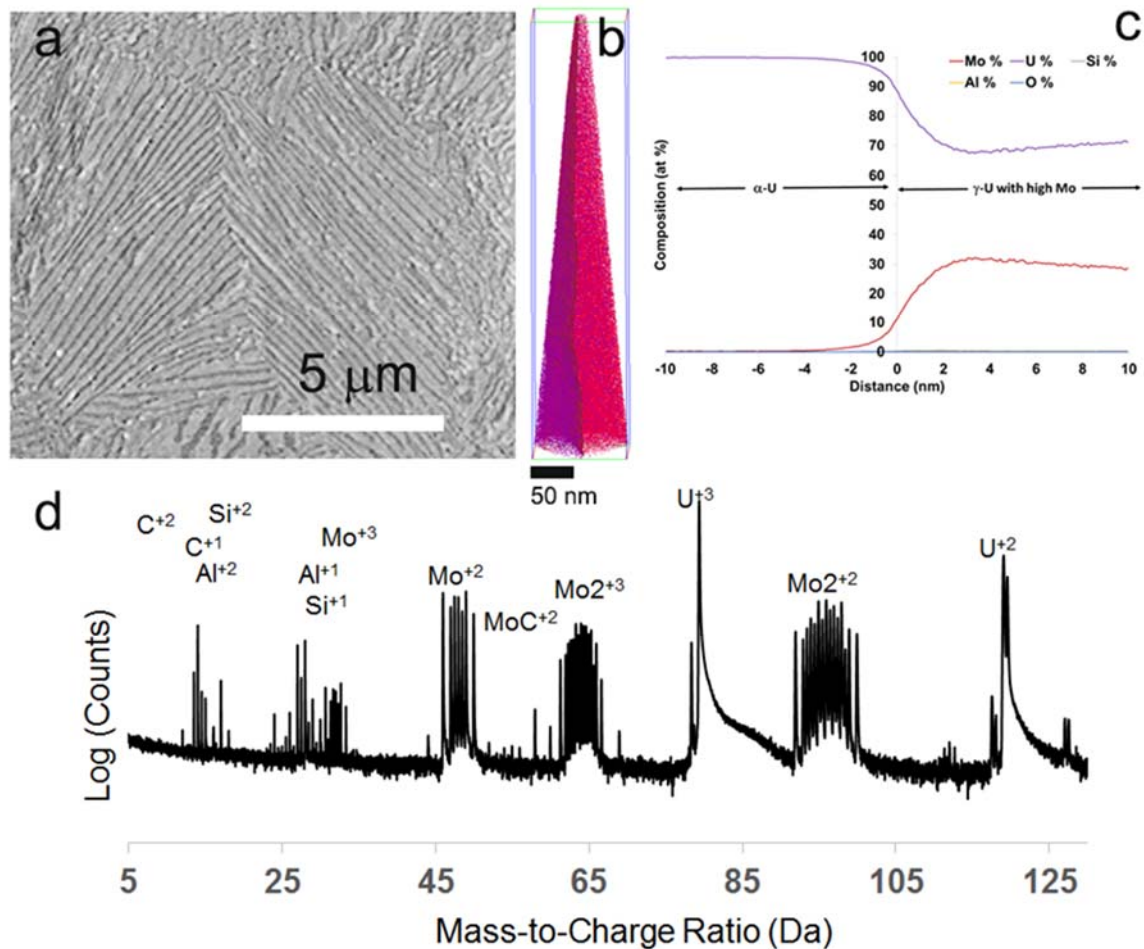


Figure 14. Transformed Regions in a U-10Mo Alloy Isothermally Aged at 500°C for 10 Hours. (a) SEM image; (b) corresponding APT reconstruction; (c) composition at phase interface showing presence of α and γ phases; (d) mass-to-charge spectrum.

6.0 Conclusions

This report provided a background on the procedures for the following:

- preparation of TEM and APT samples of various microstructural features from UMo alloys in a dual-beam FIB system using a site-specific lift-out process
- TEM imaging and diffraction of UMo alloys along with reference SAD patterns for all the common phases expected to be present in UMo alloys for main SAD zone axes
- analysis of the nanoscale composition of microstructural features including individual phase composition and interface compositions in UMo alloys by APT.

7.0 Recommendations

Detailed characterization methods like TEM and APT can provide a more comprehensive understanding of U-10Mo alloy microstructure, beyond what could be achieved by SEM and OM or XRD methods alone. Often such detailed microstructural investigation provides information that is not otherwise available due to the ultrahigh spatial resolution and sensitivity needed for composition or structure measurements. Careful attention must be paid in down-selecting representative regions of the microstructure to conduct detailed characterization investigations by TEM and APT. The detailed characterization methods also should be repeated on samples from a few different regions of the sample to develop statistical confidence in the findings achieved, especially to account for variabilities known to exist during the UMo casting process, such as melt turbulence during mold filling. Through this report, we have highlighted the unique instrumentation and expertise available at PNNL for comprehensive detailed microstructural characterization of U-10Mo fuels, which can play a critical role in accurately understanding the influence of various steps in the UMo process flow on UMo microstructure. Ultimately, we also anticipate that detailed microstructural characterization will help in tailoring processing to achieve cost reduction during various stages of fuel process flow as well as finally achieve even better irradiation performance for the final fuel form.

8.0 References

Devaraj A, VV Joshi, S Jana, L Sweet, C Mcinnis, S Manandhar, and CA Lavender. 2016. *Detecting the Extent of Eutectoid Transformation in U-10Mo*. PNNL-SA-120714, Pacific Northwest National Laboratory, Richland, WA.

Jana S, V Joshi, A Devaraj, L Kovarik, LE Sweet, S Manandhar, T Varga, and C Lavender. 2016. *Phase Transformation Kinetics in a U-10wt%Mo Cast, Homogenized Alloy at 500°C and 400°C*, PNNL-25990, Pacific Northwest National Laboratory, Richland, WA.

Prabhakaran R, VV Joshi, MA Rhodes, AL Schemer-Kohrn, AD Guzman, and CA Lavender. 2016. *U-10Mo Sample Preparation and Examination using Optical and Scanning Electron Microscopy*. PNNL-25308, Pacific Northwest National Laboratory, Richland, WA.



Pacific Northwest
NATIONAL LABORATORY

*Proudly Operated by **Battelle** Since 1965*

902 Battelle Boulevard
P.O. Box 999
Richland, WA 99352
1-888-375-PNNL (7665)

U.S. DEPARTMENT OF
ENERGY

www.pnnl.gov